SAND2013-10701C

A Computational Approach to Simulating the Effects of Realistic Surface Roughness on Boundary Layer Transition

Christopher M. Langel*, Raymond Chow†, and C.P. van Dam‡
University of California, Davis, Davis, CA 95616

David Maniaci§
Sandia National Laboratories, Albuquerque, NM 87185

Robert S. Ehrmann¶ and Edward B. White‖
Texas A&M University, College Station, TX 77843

A surface roughness model extending the Langtry-Menter transition model has been implemented in a RANS framework. The model, originally proposed by Dassler, Kozulovic, and Fiala, introduces an additional scalar field roughness amplification quantity. This value is explicitly set at rough wall boundaries using surface roughness parameters and local flow quantities. This additional transport equation allows non-local effects of surface roughness to be accounted for downstream of rough sections. This roughness amplification variable is coupled with the Langtry-Menter model and used to modify the criteria for transition. Results from flat plate test cases show good agreement with experimental transition behavior on the flow over varying sand grain roughness heights. Additional validation studies were performed on a NACA 0012 airfoil with leading edge roughness. The computationally predicted boundary layer development demonstrates good agreement with the experimental results. New experimental tests using multiple roughness configurations were conducted to further validate and calibrate the model. Finally modifications are discussed to potentially improve the behavior of the Langtry-Menter transition model at high Reynolds numbers and angles of attack.

I. Introduction

A. Motivation

The effect of surface roughness on the flow over a contaminated surface has been studied for almost a century, and there have been a large number of experimental studies that document how roughness changes observable flow properties.[1] However, a comprehensive analytical description or even a robust and effective computational method to predict detailed flow behavior over a rough surface has eluded the engineering and scientific communities. The role of surface roughness in many flow applications is of great practical importance as a well known effect is the acceleration of the laminar-turbulent transition process.[2,3] The implications of the premature appearance of turbulent flow are vast due to the changes in the aerodynamic, heat transfer, and gas mixing properties. There is an interest in understanding the effects of surface roughness across many engineering disciplines, including the effects seen in gas turbines to better approximate maintenance cycles,[4] applications to icing effects seen on aircraft wings,[5] combustion analysis, and more.

*Graduate Student Researcher.
†Postdoctoral Scholar.
‡Professor & Chair, Associate Fellow AIAA.
§Senior Member of Technical Staff.
¶Graduate Research Assistant, AIAA Student Member.
‖Associate Professor, Associate Fellow AIAA.

The wind industry in particular has seen a recent rise in interest regarding the effects of surface roughness for several reasons.[6] For one, accurate prediction of wind turbine power output is fundamental to integration of wind power systems into existing infrastructure. The changes in the flow over rough portions of a turbine blade extends to the performance of the full turbine, potentially reducing power output and annual energy capture significantly.[7] Additionally many airfoils intended specifically for use on utility scale wind turbine were designed to be lift insensitive to surface roughness due to the expected environmental conditions. As field observations are showing this is frequently not the case, there is a renewed interest in examining roughness sensitivity for airfoil design.[6,8]

The inclusion of roughness sensitivity to airfoils and other flow control surfaces poses numerous challenges due to the limited number of roughness configurations that have been thoroughly analyzed, and the non trivial extension of roughness effects. As physically testing each profile is not practical, numerical optimization methods are used to generate ideal airfoils and other flow control surfaces. However there are limited computational techniques availible to analyze the effects that surface roughness will have on the aerodynamic properties.[6,8] For the purpose of both prediction of flows over existing rough surfaces and roughness insensitive designs, a robust computational method that predicts the effects of various surface roughness distributions is strongly desired.

B. Roughness Effects

A primarily studied effect of surface roughness is the premature transition of a laminar boundary layer to a turbulent profile.[3,9] Even more effects are seen as a fully developed turbulent boundary layer has a tendency to thicken over rough sections. This is due to the increase in turbulent fluctuations and subsequent turbulent kinetic energy production over rough surfaces. The early onset of transition and modifications to the fully turbulent boundary layer on an airfoil can increase drag, alter stall characteristics, change the lift-curve slope, and even force the flow unsteady.

A crucial component is characterization of the roughness such as the height, shape, and distribution. All must all be taken into consideration to fully understand the effects. The relationship between the height of the roughness element and the flow disturbance induced is not easily correlated.[10] Roughness elements shorter than the height of the viscous sublayer generally have little effect on the transition process as the disturbances are dissipated away due to the high levels of viscous damping. Additionally as the boundary layer does not have a constant thickness, the effects can not be generalized along the boundary layer of a rough surface.[11] Accordingly, roughness heights are usually non-dimensionalized with respect to the displacement thickness (k/δ^*) or described using a roughness Reynolds number, Re_k. The roughness Reynolds number is defined:

$$Re_k = \frac{\rho U_k k}{\mu} \tag{1}$$

where U_k represents the velocity in an undisturbed boundary layer at height, k. Due to the U_k term, even if the height of the roughness remains constant, Re_k will change along a surface as the boundary later develops. Frequently, experimental studies have attempted to identify a critical Reynolds number, $Re_{k,crit}$.[2] The value of Re_k that if obtained on a rough surface will immediately trigger the transition process at that location. As many external factors such as freestream turbulence, acoustic noise, and crossflow contamination can alter transition characteristics $Re_{k,crit}$ values inherently contain some tolerance.

Roughness distributions can be broadly classified into three different subsets: 2D roughness (such as a trip strip or step), isolated 3D rough element, and distributed roughness, encompassing any grouping of rough elements and inherently 3D. Different types of roughness are known to alter the transition process uniquely, and therefore have differing $Re_{k,crit}$ values. 2D roughness is known to amplify the naturally occurring Tollmien-Schlichting wave dominated transition process by introducing a Rayleigh instability and can act to progressively move the transition location upstream.[12] A Re_k of 25-50 is taken as $Re_{k,crit}$ for 2D roughness. Isolated 3D roughness introduces flow structures known as horseshoe and hairpin vortices. These vortices remain relatively stable and have little effect on the transition process until the height of the roughness reaches a point where transition location moves rapidly upstream.[13] Due to this phenomena, isolated 3D roughness is considered to behave more "critically" than 2D. Isolated 3D roughness elements have an $Re_{k,crit}$ between 400-600 depending on the shape and height to diameter ratio.[13]

Distributed roughness becomes more difficult to quantify, one height parameter (k) is no longer enough to fully describe the roughness and its respective effects on the transition process. Several attempts have

been made to correlate measurable parameters to an equivalent sand grain roughness heights (k_s). A review conducted by Bons[4] provides the details of many efforts to create an equivalent k_s value given certain quantifiable parameters. Furthermore, the exact mechanism by which distributed roughness alters transition characteristics remains misunderstood. Several conjectures have been made as to how distributed roughness promotes the transition process. These include streamwise vortex structures produced in a similar manor to isolated 3D elements, increased receptivity of the low inertia fluid in between the rough elements, and vertical transfer of u-momentum altering the mean profile. Despite challenges in identifying exactly how the transitions process is accelerated $Re_{k,crit}$ values of 600 for distributed roughness have been used to a reasonable degree of accuracy.[3]

II. Computational Methods for Transition Prediction

A common engineering approach to analyzing complex flow problems is the use of Reynolds-averaged Navier-Stokes (RANS) simulations. Fundamentally RANS procedures require the use of a complementary closure or turbulence model to fully represent practical flows. Unfortunately these models fail to account for many physical mechanisms that cause a boundary layer to transition from laminar to turbulent. This is not easily corrected as many factors can ultimately cause the breakdown of a laminar boundary layer into a characteristic turbulent form.

Historically several methods have been used to quantify the criteria necessary for a boundary layer to begin transition. Stability based techniques such as the e^N method of Smith and van Ingen[14] have proven to accurately represent natural transition, however implementation into RANS codes requires extremely fine near wall grid resolution and the computation of integral values, restricting use in general purpose CFD codes. Disturbance growth rate methods for transition prediction have also been implemented by Brodeur and van Dam,[15] and Mayda.[16] However, these techniques suffer from similar incompatibilities as the e^N method when applied to general purpose RANS codes. A recently developed alternative approach is that of local correlation-based transition modeling (LCTM).[17,18] The general concept is to introduce an empirically correlated quantity based on freestream values that is subsequently compared to local flow conditions and used to indicate when the flow begins to transition. A primary appeal is that LCTMs are designed to predict boundary layer transition entirely based on local flow quantities allowing parallelization and use on unstructured grids.[18]

A. Langtry-Menter $\gamma - \tilde{Re}_{\theta t}$ Model

Correlation based transition prediction methods rely heavily on a non-dimensional form of the boundary layer momentum thickness ($Re_\theta = \rho\theta/\nu$) and its relation to the stability of the boundary layer. In a similar manner to the e^N process, a fully laminar solution is initially assumed and the momentum thickness Reynolds number (Re_θ) is computed at all locations. The Re_θ values are then compared to an empirical correlation, e.g. Abu-Ghannam and Shaw,[19] to determine the location of the onset of transition. However typically the computation of θ requires both an integration and the definition of a boundary layer edge, both non-local operations. To localize the computation, Menter and Langtry introduced the relationship between Van Driest and Blumers[20] vorticity Reynolds number (Re_ν) and Re_θ. The vorticity or likewise known strain-rate Reynolds number is defined:

$$Re_\nu = \frac{\rho y^2}{\mu}\left|\frac{\partial u}{\partial y}\right| = \frac{\rho y^2}{\mu}S \tag{2}$$

Although not an entirely local quantity the wall distance can be computed using a Poisson equation when not directly available from the grid topology. In the transition model Re_ν is related to Re_θ by the following:

$$Re_\theta = \frac{\max(Re_\nu)}{2.193} \tag{3}$$

The $\max(Re_\nu)$ corresponds to the maximum value the vorticity Reynolds number obtains in the plane normal to the surface. The denominator is chosen to be 2.193 such that for a Blasius profile $\max\{(2.193Re_\theta)/Re_\nu\} = 1$. Along with the procedure to compute the local Re_θ without having to perform any integrations a transport equation is used to distribute the empirical correlation throughout the flow field to facilitate the comparison between the local Re_θ and a localized onset value. The model, referred to as the Langtry-Menter $\gamma - \tilde{Re}_{\theta t}$

model, defines the "transition onset momentum thickness Reynolds number" ($\tilde{Re}_{\theta t}$) to serve as the onset criteria. $\tilde{Re}_{\theta t}$ is determined by the equation:

$$\frac{\partial(\rho\tilde{Re}_{\theta t})}{\partial t} + \frac{\partial(\rho U_j \tilde{Re}_{\theta t})}{\partial x_j} = P_{\theta t} + \frac{\partial}{\partial x_j}\left[\sigma_{\theta t}\left(\mu + \mu_t\right)\frac{\partial \tilde{Re}_{\theta t}}{\partial x_j}\right] \tag{4}$$

The production term contains the empirical correlation, referred to as $Re_{\theta t}$. The function is defined:

$$P_{\theta t} = c_{\theta t}\frac{\rho}{t}(Re_{\theta t} - \tilde{Re}_{\theta t})(1 - F_{\theta t}) \tag{5}$$

$Re_{\theta t}$ is a direct computation of the correlation, while $\tilde{Re}_{\theta t}$ is determined purely by the transport equation to account for localized effects. Once the distribution of $\tilde{Re}_{\theta t}$ is determined an intermediate value is computed referred to as the "critical momentum thickness Reynolds number," $Re_{\theta c}$. The parameter is defined such that $Re_{\theta c} = f(\tilde{Re}_{\theta t})$, and determines the value the vorticity Reynolds number must obtain to trigger intermittency (γ) production. The production of intermittency attempts to simulate the transition process by progressively switching on the underlying SST $k-\omega$ turbulence model. The distribution of intermittency is governed by a second transport equation:

$$\frac{\partial(\rho\gamma)}{\partial t} + \frac{\partial(\rho U_j \gamma)}{\partial x_j} = P_\gamma - E_\gamma + \frac{\partial}{\partial x_j}\left[\left(\mu + \frac{\mu_t}{\sigma_f}\right)\frac{\partial \gamma}{\partial x_j}\right] \tag{6}$$

The value of intermittency in the freestream is set to 1, this differs form the usual definition where an intermittency of 1 is reserved for a fully turbulent state. This is necessary to accurately account for freestream turbulence decay rates and to allow the SST $k-\omega$ turbulence model to function undisturbed outside the boundary layer. Additionally, even though it is not shut off directly using the intermittency variable, production of turbulent kinetic energy is limited in the freestream if there is a lack of shearing stress in the mean flow. E_γ is included in the intermittency transport equation to account for the possibility of re-laminarization under the influence of a highly favorable pressure gradient.

The production term (P_γ) is given by:

$$P_\gamma = F_{length} c_{a1} \rho S [\gamma F_{onset}]^{\frac{1}{2}} (1 - c_{e1}\gamma) \tag{7}$$

c_{e1} and c_{a1} are model constants and S is the magnitude of the strain rate, F_{length} is calibrated based on the benchmark ERCOFTAC[21] and Schubauer and Klebanoff[22] flat plate test cases, and controls the rate at which the turbulent boundary layer develops. The function F_{onset} acts to compare Re_ν and $Re_{\theta c}$ and is strongly dependent on the F_{onset1} function defined:

$$F_{onset1} = \frac{Re_\nu}{2.193 \cdot Re_{\theta c}} \tag{8}$$

Once the onset criteria as been met the intermittency variable is used to progressively activate k production by scaling the production term in the SST-$k-\omega$ turbulence model.

$$\frac{\partial(\rho k)}{\partial t} + \frac{\partial(\rho U_j k)}{\partial x_j} = \tilde{P}_k - \tilde{D}_k + \frac{\partial}{\partial x_j}\left[\left(\sigma_k \mu_t + \mu\right)\frac{\partial k}{\partial x_j}\right] \tag{9}$$

with,

$$\tilde{P}_k = \gamma_{eff} P_k; \qquad \tilde{D}_k = \min(\max(\gamma_{eff}, 0.1), 1.0) \cdot D_k \tag{10}$$

where γ_{eff} is defined as $\max\{\gamma_{sep}, \gamma\}$ to allow the model to rapidly induce k production if the flow separates. A more detailed description of the separation caused trigger (γ_{sep}) and full equation set is presented in Langtry and Menter.[18]

B. OVERFLOW-2

OVERFLOW-2 is a structured overset, unsteady Reynolds-averaged Navier-Stokes flow solver. As a flow solver, it is very robust and comprehensive, allowing for the selection from a variety of numerical schemes, turbulence models, boundary conditions, and time advancement schemes.[23] Due to extensive capabilities and accessibility of the source code, OVERFLOW-2 was selected as a base for the computational roughness model to be implemented.

C. Freestream Turbulence Decay

The Langtry-Menter transition model was developed for use in the code ANSYS-CFX, and the correlation functions left proprietary in the initial publication of the methodology. The full equation set was then published in 2009[18] and subsequently coded into the latest release of OVERFLOW-2, version 2.2e. In the process of running flat plate validation cases with OVERFLOW-2 a number of issues arose regarding the freestream turbulence intensity parameter (FSTI). Large discrepancies in the FSTI between the grid inflow where it is prescribed and the leading edge of the flat plate were observed. This decay is associated with lack of proper grid resolution in the inflow section of the computational grid giving rise to unphysical numerical dissipation. As the transition correlation in the Langtry-Menter model is a strong function of FSTI, the decay nullified the models ability to predict the free-transition location on the flat plate test cases (See Figure 1). Fortunately under the influence of a strong pressure gradient it was observed the model demonstrated less sensitivity to FSTI, nonetheless the issue of freestream turbulence decay is of great importance.

Two different methods to remedy the unphysical drop in FSTI were explored in the current study. The first followed a suggestion by Spalart and Rumsey to impose floor values on the decay rate of ω.[24] This was done in OVERFLOW-2 by modifying the destruction term of the original ω-transport equation:

$$D_\omega = \beta\rho\omega^2 \tag{11}$$

modified to:

$$\tilde{D}_\omega = \beta\rho(\omega - C_\omega) \tag{12}$$

with C_ω the freestream turbulence decay rate. In effect, the the limiter switches off the decay near inviscid walls due to discrepancies in the magnitude of ω near viscous and inviscid walls. However, as the modification is to the turbulence model directly the change is not purely limited to the inviscid section so there is a slight change in the model globally.

The other approach taken to resolve the issue of freestream decay was to create separate computational grids for the inflow and the viscous flat plate section and combine the two domains using overset grid techniques. In separating the grids by oversetting separate boundary and flow conditions can be prescribed allowing an inviscid solution to be imposed in the inflow region. This effectively translates the freestream turbulence conditions to the leading edge of the flat plate eliminating the inflow decay issue altogether.

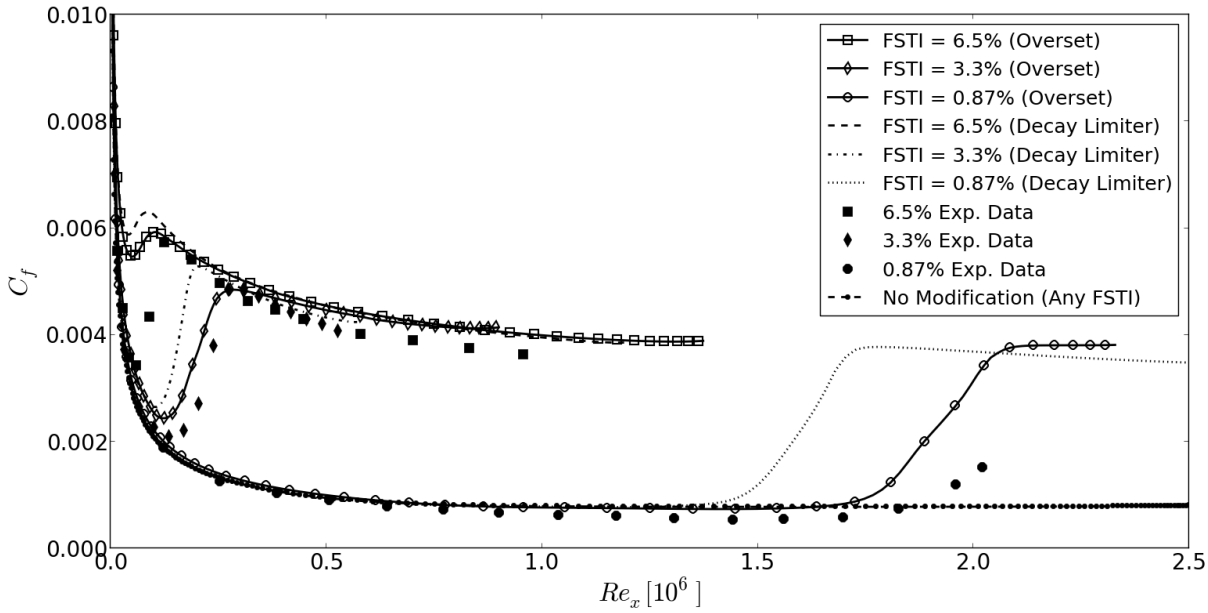

Figure 1: Plot of skin friction obtained using the two techniques for reducing the error introduced by unphysical numerical dissipation in the inflow, unmodified case also shown

As seen in Figure 1 both methods produce a better solution than without any modification, though oversetting the grids agrees better with the experimental results at all freestream turbulence levels. The

overset method is advantageous as it can also be applied to airfoil and other more geometrically complex cases by splitting the grid into a near-body and far field section and imposing an inviscid solution off body.

III. Roughness Amplification Model

Computationally attempts at roughness modeling have generally followed three approaches: (1) Modifying the turbulent eddy viscosity near wall in accordance to the relative height of the roughness. (2) Modify the governing flow equations directly to account for blockage effects and momentum loss due to increased drag. (3) Discretely model the rough features using an ultra fine near wall mesh. Due to the impractically high grid generation and computational costs, the option of discretely modeling the roughness is rarely taken.[4] Adding terms to the governing equations to account for the macroscopic physical behavior does have advantages, however small miscalculations can severely effect the accuracy of the flow solution. Modifying near wall turbulent behavior by adjusting parameters in the turbulence model is a popular approach and several strategies have been implemented by Durbin[25] and Hellsten and Laine.[26] A similar approach is taken in the current work and discussed further in section III.B. While the modifications to the turbulence model boundary conditions can adjust the mean profiles once the boundary layer has fully transitioned, the acceleration of the transition process requires additional considerations.

In an attempt to include the influence of surface roughness on boundary layer transition in a purely computational manner, Dassler, Kozulovic, and Fiala[27,28] introduced a third term to the Langtry-Menter model. The "Roughness Amplification" (A_r) variable is treated as an additional non-physical quantity that will be produced at rough surface boundaries. Using a scalar transport equation the variable is convected into the flow field and defines a region of roughness influence to locally modify the transition model downstream of a rough section. The variable attempts to represent the build up of roughness induced perturbations and modify the criteria for transition onset accordingly.

A. Roughness Model Background

The behavior of the Langtry-Menter transition model is strongly dependent on the momentum thickness of the boundary layer. Under similar freestream conditions, the higher the boundary layer momentum thickness the more unstable the boundary layer becomes. Surface roughness has been reported to cause an increase in the momentum deficit over rough sections, and as a result increase the momentum thickness. This change will alter the correlation in the transition model as in principle it computes an estimate of the momentum thickness Reynolds number along a streamline and seeks a critical value as determined by the transport equation for $\tilde{R}e_{\theta t}$. The option for modifying the correlation to account for roughness is to either increase the locally computed Re_θ or lower the critical value, $\tilde{R}e_{\theta t}$, it must obtain in the region effected by the surface roughness.

An indication of the momentum loss can be determined using the variable k^+, defined:

$$k^+ = \sqrt{\frac{\tau_w}{\rho_w}} \cdot \frac{k_s}{\nu} \tag{13}$$

The dependence on wall shear stress, τ_w, provides the velocity gradient at the wall and combined with the roughness height can be used to roughly approximate the momentum deficit behind the roughnesss element. To bring in some empiricism there is a relation between k^+ and Re_k where:

$$k^+ \approx \sqrt{Re_k} \tag{14}$$

This relation can be derived by assuming a linear varying near wall velocity such that:

$$u(z) = \frac{\tau_w z}{\mu} \tag{15}$$

and substituting Eq. 15 in the expression for Re_k. This allows a calibration based on the experimentally determined $Re_{k,crit}$ values for various roughness configurations.

To determine how the A_r variable should interact with the transition model, a brief analysis of how the roughness will effect the momentum thickness was performed. Once more assuming a linearly varying near wall velocity and incompressibility Eq. 15 can be inserted into the expression for the computation of

momentum thickness. The change in θ, and therefore Re_θ, can be approximated by integrating up to the height of the roughness:

$$\Delta\theta = \int_0^{k_s} \frac{u(z)}{u_0}\left(1 - \frac{u(z)}{u_0}\right) dz \tag{16}$$

If the integration is carried out with Eq. 15 used as $u(x)$ the resulting change in Re_θ can be written in terms of k^+:

$$Re_{\theta,rough} = Re_\theta + \frac{1}{3}u^+(k^+)^3 - \frac{1}{2}(k^+)^2 \tag{17}$$

with $u^+ = u/u_\tau$.

The goal of the A_r variable is to trigger the transition process with a smaller disturbance. This can be accomplished by using the variable to increase the local momentum thickness Reynolds number Re_θ, or lower the correlated critical value by a similar amount. The option taken is to decrease the local correlation variable $\tilde{R}e_{\theta t}$ by modifying the production term in the transport equation. The reason for this is the computation of the local momentum thickness number is based on a relationship to Re_ν rather than a direct computation.

The distribution of A_r is determined using an additional scalar transport equation that takes a similar form to those of the transition model:

$$\frac{\partial(\rho A_r)}{\partial t} + \frac{\partial(\rho U_j A_r)}{\partial x_j} = \frac{\partial}{\partial x_j}\left[\sigma_{ar}\left(\mu + \mu_t\right)\frac{\partial A_r}{\partial x_j}\right] \tag{18}$$

The form of the equation allows time histories of increased turbulent kinetic energy production to be convected away from the roughness itself and can be calibrated to produce the experimentally observed[19] lag between encountering the rough section and the effects seen on boundary layer flow. The A_r equation does not include an explicit production term, alternatively the distribution of A_r is determined with a boundary condition at rough walls where the user inputs a representative equivalent sand grain roughness height (k_s). As discussed the primary factor influencing the value of A_r at rough walls is the dimensionless sand grain roughness, k^+.

Upon computation of k^+ the value of A_r at the rough wall boundary is define $A_r|_{wall} = c_{Ar1}k^+$. With the boundary condition and transport equation the distribution is defined for the entire flow field. The interaction with the Langtry-Menter model is through the production term for $\tilde{R}e_{\theta t}$. Originally defined as:

$$P_{\theta t} = c_{\theta t}\frac{\rho}{t}(Re_{\theta t} - \tilde{R}e_{\theta t})(1 - F_{\theta t}) \tag{19}$$

The modified $P_{\theta t,mod}$ equation becomes:

$$P_{\theta t,mod} = c_{\theta t}\frac{\rho}{t}\left[(Re_{\theta t} - \tilde{R}e_{\theta t})(1 - F_{\theta t}) - F_{A_r}\right] \tag{20}$$

It can be seen the interaction of F_{Ar} with the transition model is to drive down the local $\tilde{R}e_{\theta t}$ downstream of rough sections, where high levels of A_r occur. The F_{A_r} expression is a cubic based on the result of Eq. 17 and that $A_r = c_{Ar1}k^+$ at a rough wall.

$$F_{A_r} = \begin{cases} c_{Ar2}\cdot(A_r)^3 & : A_r < C_{A_r} \\ c_{Ar3}(A_r - C_{A_r}) + c_{Ar2}C_{A_r}^3 & : A_r \geq C_{A_r} \end{cases} \tag{21}$$

In lowering $\tilde{R}e_{\theta t}$, the value the local strain rate must obtain to trigger intermittency production will ultimately be decreased, and therefore the onset of transition will occur with smaller flow disturbances. The current model parameters used in for the test cases presented are:

$$c_{Ar1} = 8.0 \qquad c_{Ar2} = 0.0005 \qquad c_{Ar3} = 2.0 \qquad \sigma_{ar} = 10.0$$

The function is switched at $C_{A_r} = \sqrt{c_{Ar3}/3c_{Ar2}}$ to allow the smooth transition between the cubic and linear functions.

B. Modified SST $k-\omega$ Boundary Conditions

In addition to modifying the transition model an update is proposed to account for the effects of surface roughness on the fully transitioned boundary layer. The modification is a change to the boundary conditions in the original SST model, representing the lowering of the turbulent dissipation rate (ω) at rough walls. The original boundary condition:

$$\omega_{smooth} = 10\frac{6\nu}{\beta(\Delta y)^2} \quad \text{with} \quad \beta = 0.09 \quad \text{at} \quad y = 0 \tag{22}$$

where Δy represents the normal distance from the wall to the nearest grid point.

The update to account for roughness, originally proposed by Wilcox:[31]

$$\omega_{rough} = \frac{\mu_\tau^2 S_r}{\nu} \quad \text{with} \quad \mu_\tau = \sqrt{\frac{\tau_w}{\rho_w}} \quad \text{at} \quad y = 0 \tag{23}$$

where S_r is dependent on the non-dimensional k^+ value.

$$S_r = \left(\frac{50}{k^+}\right)^2 \quad \text{if} \quad k^+ \leq 25 \tag{24}$$

$$S_r = \frac{100}{k^+} \quad \text{if} \quad k^+ > 25 \tag{25}$$

The modified boundary conditions allow the model to not only account for roughness induced transition, but also the effects on the fully turbulent boundary layer, including the increase in local skin friction.

IV. Roughness Model Implementation

For this study the aforementioned roughness amplification model has been implemented in OVERFLOW-2. For all cases the primary flow variables are calculated with sixth-order central differencing using the approximate-factorized form of the Beam-Warming pentadiagonal scheme.[30] The spatial fluxes of the roughness model are discretized using a modified Harten-Lax-van Leer (HLLC) upwind scheme as extension of the existing Langtry-Menter model with the linear matrix solved using a similar successive symmetric over relaxation (SSOR) algorithm.

A. Flat Plate Distributed Roughness

To provide a baseline for the effects of distributed surface roughness, the model has been re-calibrated on several flat plate test cases in comparison with the experimental results of Feindt[29] and the original CFD model results of Dassler, Kozulovic, and Fiala.[28] Roughness is characterized by equivalent sand grain roughness height (k_s) and the corresponding non-dimension sand grain Reynolds number $Re_{k_s} = (\rho U_k k_s/\mu)$. With U_k the velocity at the top of the roughness element as defined above. Three different pressure gradients are simulated using the grid geometry. A baseline test with no pressure gradient, along with an adverse and favorable pressure gradient. The profile of the upper wall is determined with the function:

$$r(x) = \sqrt{\frac{r_0^2}{\sqrt{1.0 - PG}}} \quad \text{with} \quad PG = \frac{p_1(x) - p_0}{q_0} \tag{26}$$

Where r_0 represents the distance from the flat plate to the upper wall at the inlet, p_0 and q_0 the static and dynamic pressure at the inlet respectively, and p_1 the static pressure along the plate. The PG parameter was set to match the conditions in the Feindt experiment for the two non-zero pressure gradient tests. The initial distance from the plate to the upper wall, r_0, was set as $0.1495c$ to match the grid used in the original CFD tests of Dassler et al.[28]

Freestream turbulence levels were set according to those used in Dassler et al.[28] and are such that the smooth wall behavior matches up with the experimental results. The tests used a FSTI of 0.91% for the zero pressure gradient and adverse pressure gradient test cases. The favorable pressure gradient required a higher FSTI then the condition used in Dassler et al. to retain an accurate simulation of smooth wall transition

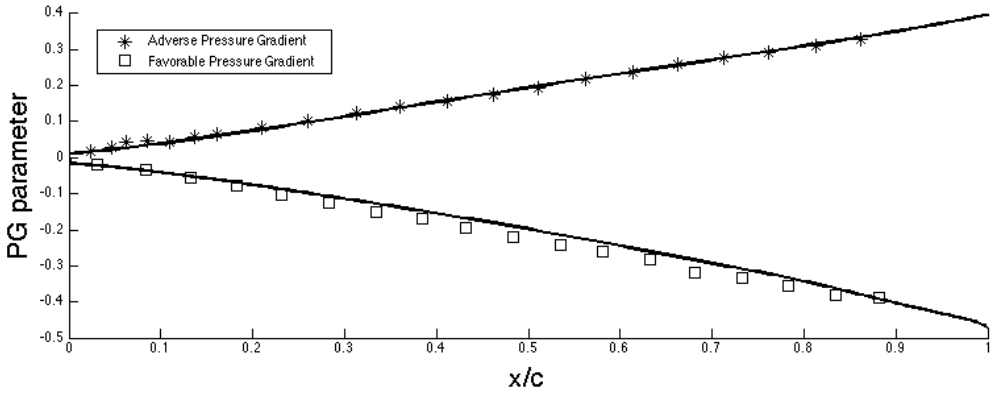

Figure 2: Plot of PG parameter used in construction of the flat plate grids, markers indicate experimental points, lines the computed pressure gradient from simulation

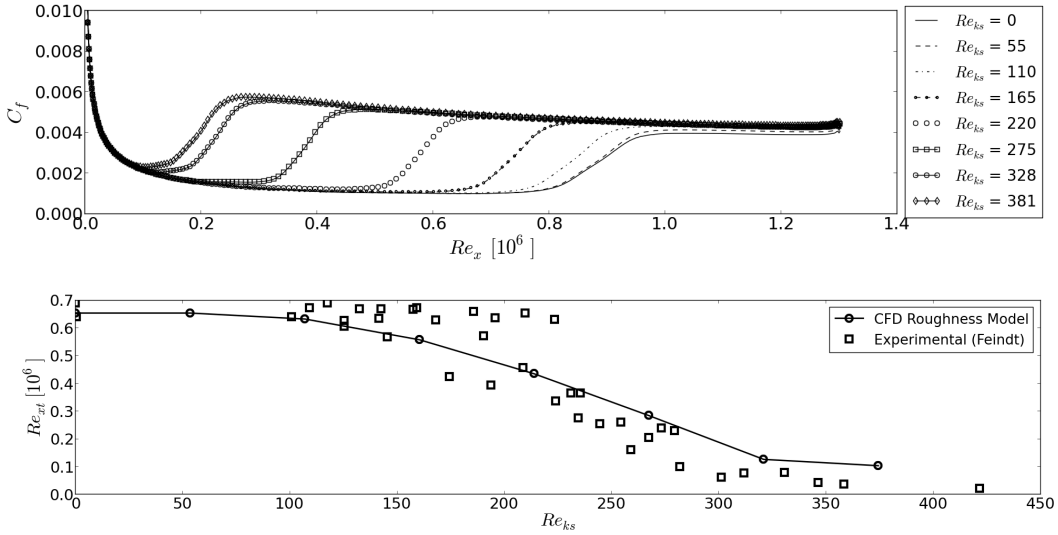

Figure 3: Flat plate with zero pressure gradient, $\alpha = 0^o$, Mach = 0.1, FSTI = 0.91%. (Top) Skin friction (C_f) for various non-dimensional sand grain roughness heights. (Bottom) Re_{ks} plotted against transition location (Re_{xt}) compared to the experimental results of Feindt.[29]

location. This could potentially be a product of the differences in implementation of the Langtry-Menter model in OVERFLOW-2 and in the code used by Dassler et al.

The effect on skin friction of varying non-dimensional sand grain roughness heights with zero pressure gradient test cases are shown in Figure 3 with transition onset defined as the streamwise location that the minimum skin friction value occurs. Furthermore, the effect of varying pressure gradients on skin friction and transition location dare shown in Figures 4 and 5. Despite the scatter and uncertainty in the experimental data, the model does a good job at predicting the overall trends under all pressure gradients. The effect of the modification to the boundary condition for ω can be seen in the modulation upward of the skin friction plots at higher roughness levels.

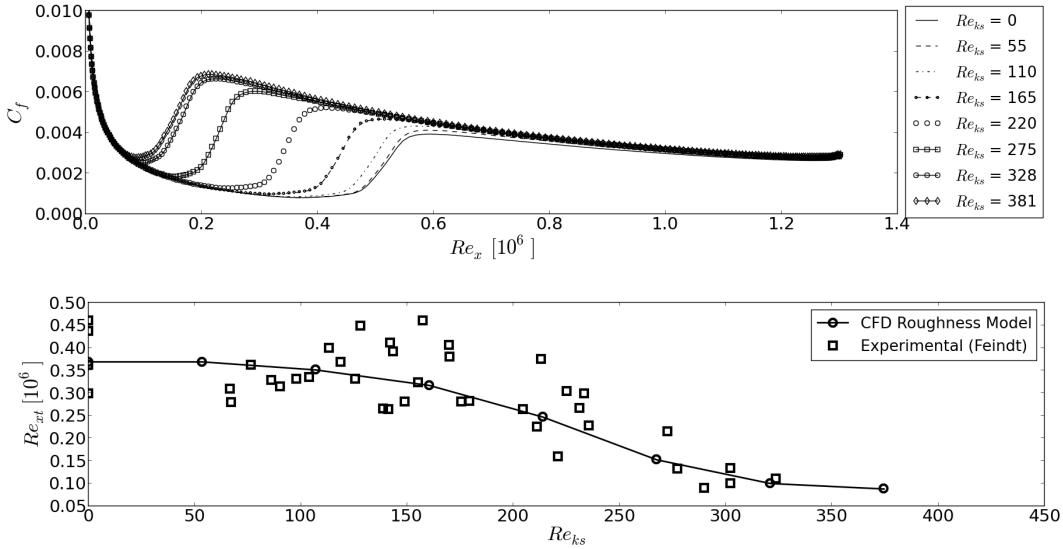

Figure 4: Flat plate with adverse pressure gradient, $\alpha = 0^o$, Mach = 0.1, FSTI = 0.91%. (Top) Skin friction (C_f) for various non-dimensional sand grain roughness heights. (Bottom) Re_{ks} plotted against transition location (Re_{xt}) compared to the experimental results of Feindt.[29]

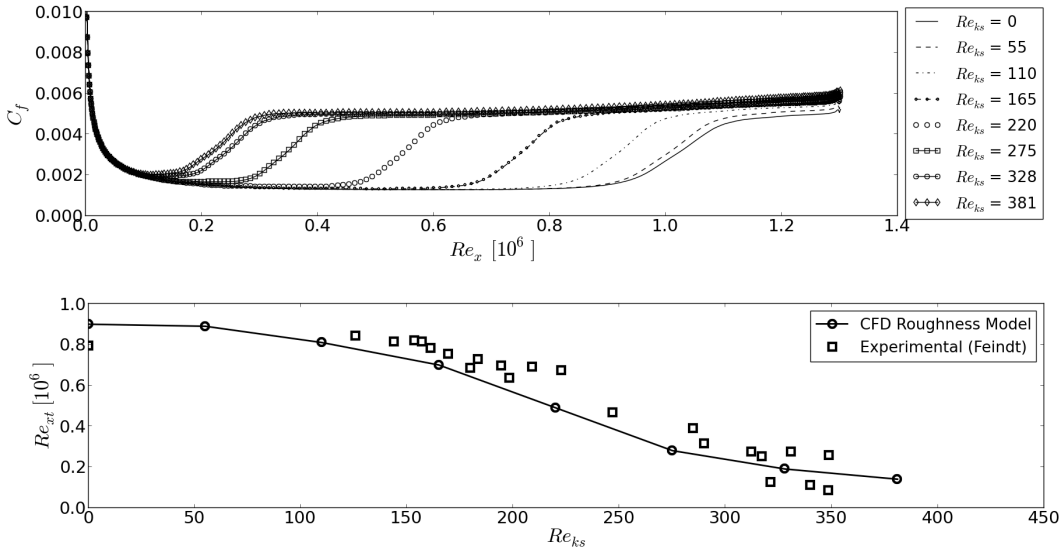

Figure 5: Flat plate with favorable pressure gradient, $\alpha = 0^o$, Mach = 0.1 , FSTI = 2.1%. (Top) Skin friction (C_f) for various non-dimensional sand grain roughness heights. (Bottom) Re_{ks} plotted against transition location (Re_{xt}) compared to the experimental results of Feindt.[29]

B. NACA 0012 with Leading Edge Roughness

The results from the flat plate test cases show good agreement with experimental results however, more complex geometries are necessary to evaluate the validity of the model. The experimental results of Kerho and Bragg were used to asses the behavior of the model applied to an airfoil with large scale leading edge erosion at varying locations and extents.[5,32] All experimental tests were performed on a NACA 0012 airfoil of chord length 0.5334 m using a tape strip with hemispherical shapes simulating distributed roughness. The roughness strips were nominally 0.35 mm high including the tape substrate and the center to center spacing of the rough elements was 1.3 mm. The authors report the location of the start of the roughness measured in mm from the leading edge center and chordwise length of the rough region in inches. More information regarding the experimental configuration can be found in Kerho and Bragg.[5] A noteworthy characteristic is the particularly high Re_k values across all test configurations. Due to these high Re_k values the test cases are useful in establishing the supercritical behavior ($Re_k > Re_{k,crit}$) of the roughness amplification model.

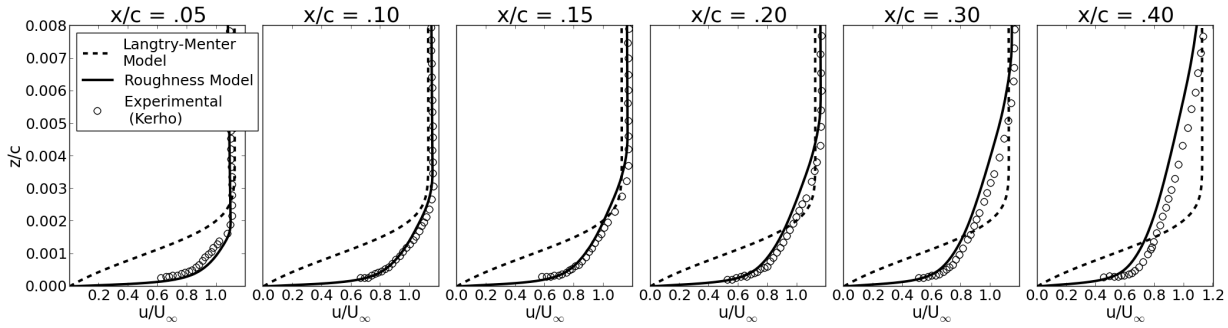

Figure 6: Boundary layer profiles with distributed roughness applied $x/c = 0.0018 - 0.0191$, Kerho,[32] unmodified Langtry-Menter transition model, computational roughness model. NACA 0012 airfoil, $Re = 1.25 \times 10^6$, $\alpha = 0^o$, FSTI = 0.1%

Boundary layer profiles from a few of the test cases are compared to the roughness model and baseline Langtry-Menter transition model to demonstrate the impact that roughness has on the development of the boundary layer. In all cases the profiles recorded from the "rough" configurations differs significantly from the clean.

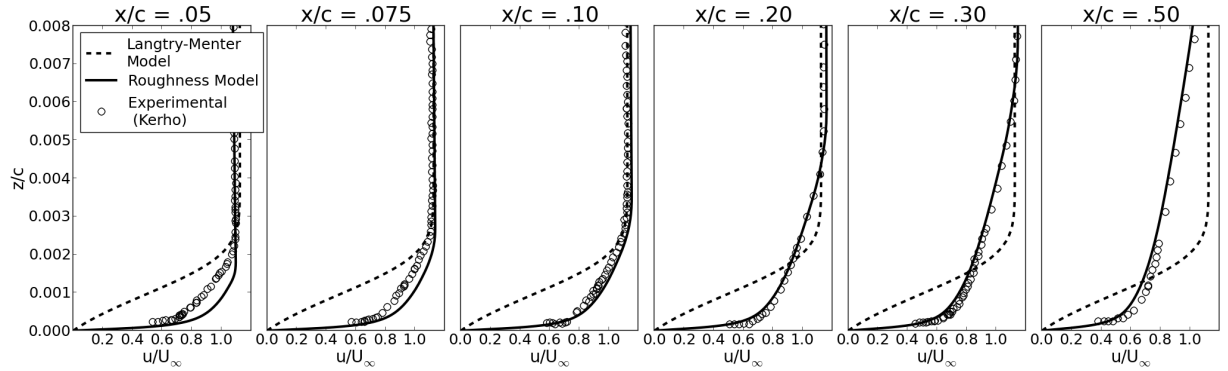

Figure 7: Boundary layer profiles with distributed roughness applied $x/c = 0.0061 - 0.0258$, Kerho,[32] unmodified Langtry-Menter transition model, computational roughness model. NACA 0012 airfoil, $Re = 1.25 \times 10^6$, $\alpha = 0^o$, FSTI = 0.1%

The first two cases (Figures 6 and 7) demonstrate significant improvement in comparison to the baseline Langtry-Menter model and match up exceptionally well compared to the experimentally measured profiles. In the test case with the roughness located furthest aft (Figure 8) the model is delays in predicting the onset of transition. A slight discrepancy is the shift in the profile seen in the more aft chord locations ($x/c = .40$ & $.50$). This is the result of a turbulent boundary layer developing too rapidly in the simulation, caused by a large production of k from the turbulence model. The trend was consistently observed across

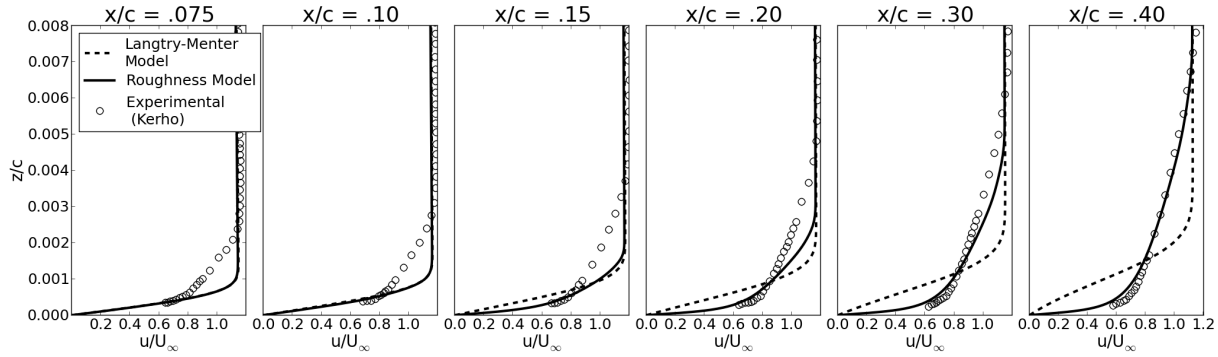

Figure 8: Boundary layer profiles with distributed roughness applied $x/c = 0.0314 - 0.0539$, Kerho,[32] unmodified Langtry-Menter transition model, computational roughness model. NACA 0012 airfoil, $Re = 1.25 \times 10^6$, $\alpha = 0^o$, FSTI = 0.1%

all roughness configurations even those which demonstrated a lag in onset prediction. As the model was calibrated using test cases that transition without the influence of roughness the inability to accurately simulate the development of a roughness induced transition is an expected consequence.

Another observation recorded by Kerho and Bragg[5] was the "state" of the boundary layer at varying chord locations for all the test configurations. The categories used to describe the boundary layers were laminar, transitional, and fully turbulent. Figure 9 shows a comparison between the experimental cases and the results from the computational model applied to an equivalent configuration. The onset of transition is defined for the experimental tests as the location the integrated intermittency profile begins to spike. Due to the nature of RANS simulations this parameter cannot be represented computationally, so the boundary layer shape factor ($H = \delta^*/\theta$) was used as indicator for the onset of transition. Typically there will be a rise in the shape factor as the laminar boundary layer grows followed by an inflection when transition begins. The criterion for fully a fully turbulent boundary layer was the chordwise location the boundary layer obtained self similarity when normalized by momentum thickness (θ) as used in the experiments.

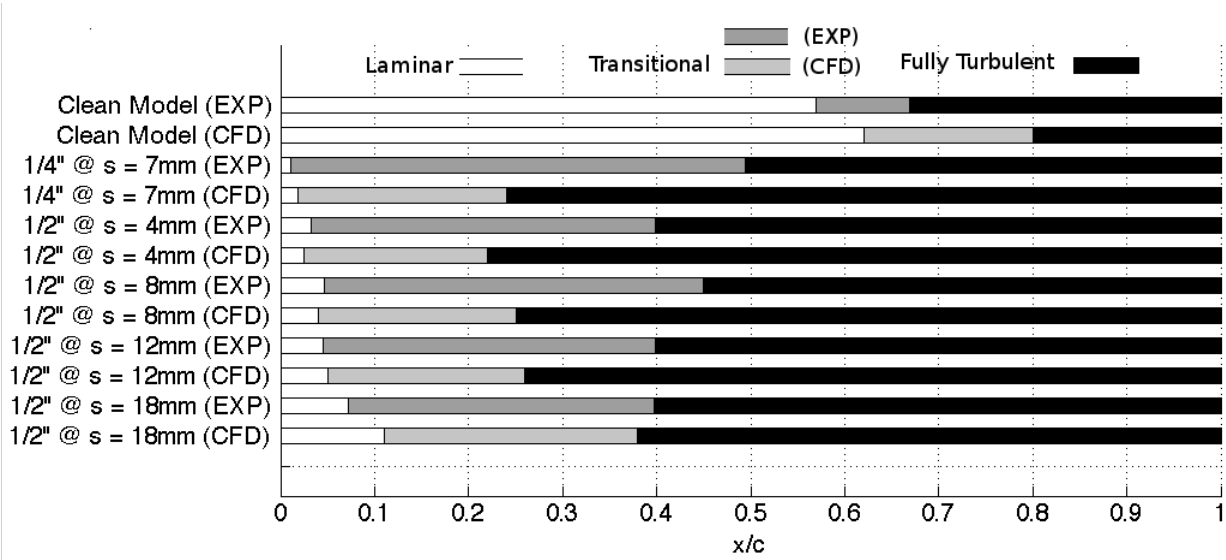

Figure 9: Comparison of boundary layer states with experimental results of Kerho and Bragg[5,32] for upper surface of NACA 0012 in clean and rough configurations, $Re = 1.25 \times 10^6$, $\alpha = 0^o$, in all test cases.

As seen in Figure 9 the model does a good job tracking the change of onset location as the location of the roughness is moved along the chord. That is the experimental test that transitions earliest is mirrored in the simulation and the relative locations of onset across the configurations match up. There is a slight delay in onset prediction in some of the cases but on the whole the model does a good job predicting the change

in onset characteristics as the location of the roughness is moved. This has very desirable implications as despite the fact the changes in the placement of roughness are relatively small the model is able to represent the movement of transition location consistently.

There is another very clear trend in Figure 9 and that is the length of the "transitional" region is repeatedly under predicted. The effects of this are visible in Figure 6 and 7 where at the latter chord regions the computational profile is shifted to the left of the experimental. An observation by Kerho was that in a roughness induced transition the max turbulent kinetic energy was actually lower than the equivalent smooth surface. This phenomena can potentially be accounted for in the F_{length} function of the Langtry-Menter model by adding A_r as a variable. This is not a trivial procedure as F_{length} and $Re_{\theta,t}$ are strongly coupled and slight changes in the F_{length} function cause large discrepancies in the global behavior of the transition model.

V. Experimental Comparison

In conjunction with the development of the computational model, wind tunnel tests on a NACA 63_3-418 airfoil with multiple roughness configurations are being carried out at the Texas A&M Oran W. Nicks Low Speed Wind Tunnel (LSWT).[33] To provide a base line the model is tested in a clean configuration, and compared to the CFD results with the unmodified Langtry-Menter transition model. The lift and drag comparisons for the clean configuration can be seen in Figure 10. There is a strong agreement between the experimental results and the CFD model for the $Re_c = 1.6 \times 10^6$ cases. As seen in Figure 10b there are a few discrepancies at the higher $Re_c = 3.2 \times 10^6$, demonstrating the sensitivity of the Langtry-Menter transition model to the freestream turbulence intensity. The LSWT reports a freestream turbulence level of 0.24%, with that parameter the $Re_c = 1.6 \times 10^6$ cases line up with the experiment while the $Re_c = 3.2 \times 10^6$ cases clearly over predict drag.

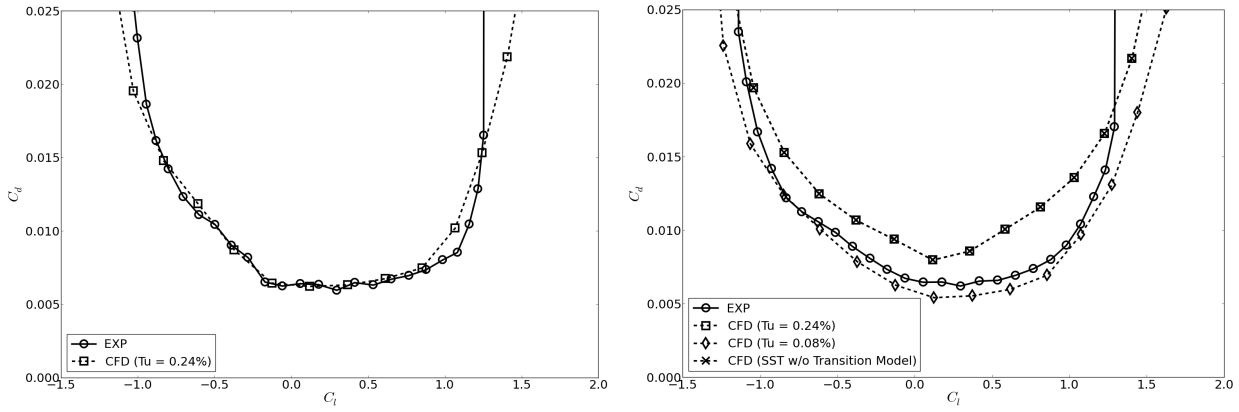

(a) $Re_c = 1.6 \times 10^6$

(b) $Re_c = 3.2 \times 10^6$

Figure 10: Drag polars for the clean configuration of a NACA $63_3 - 418$ airfoil for two Reynolds numbers with varying turbulence intensities.

A. Modifications to Onset Criteria for Langtry-Menter Model

After examining numerous results of the cases run with the Langtry-Menter model a clear trend emerges. At higher Reynolds numbers and angles of attack, the model predicts the onset of transition upstream of where the experimental results indicate. This can be seen in Figure 10b where the early onset of transition causes a rise in the drag coefficient, effectively shifting the drag curve upward.

Several researchers noted that a cause of the premature transition onset prediction was due to the function within the model that compared the strain-rate Reynolds number to the criteria for transition onset.[36] As discussed the model does not actually compute the momentum thickness of the boundary layer, but rather use the relationship between the maximal value of the strain rate Reynolds number and a calibrated constant. (see Eq. 8) The initial implementation was based off a Blasius profile with no pressure gradient where the relationship between Re_ν and the momentum thickness Reynolds number is well defined. A solution

investigated was to change the constant parameter in the F_{onset1} equation. By increasing the constant from 2.193 to 3.29, Khayatzadeh et al.[36] showed the model demonstrated less sensitivity to freestream turbulence intensity and much better agreement to experimental tests at higher Reynolds numbers and angles of attack. The modification effectively allows the boundary layer to develop further before switching the turbulence model on. The modified onset function:

$$F_{onset1,mod} = \frac{Re_\nu}{3.29 \cdot Re_{\theta c}} \tag{27}$$

The proposed modification was implemented in OVERFLOW-2 and the NACA 63_3-418 cases reanalyzed to provide a first step at accessing the validity of the change. Figure 11 shows the drag polars of the NACA 63_3-418 airfoil at $Re_c = 1.6 \times 10^6$ and 3.2×10^6 with the onset modification.

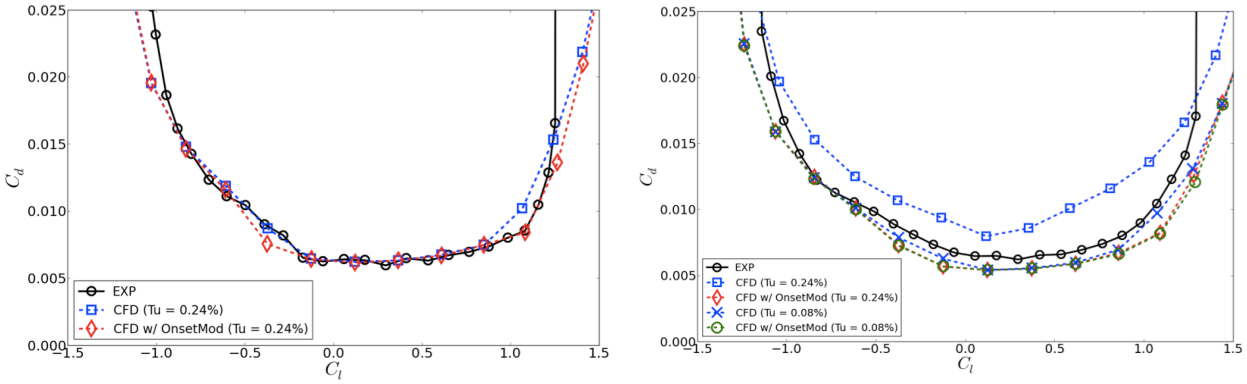

(a) $Re_c = 1.6 \times 10^6$ (b) $Re_c = 3.2 \times 10^6$

Figure 11: Drag polar of NACA 63_3-418 airfoil, Langtry-Menter transition model with onset modification and LSWT wind tunnel results

The results of modification at $Re_c = 1.6 \times 10^6$ are almost identical in the lower portion of the drag bucket, and demonstrate better agreement at higher lift coefficients and therefore angles of attack. However, around $C_l = -0.5$ the modified results actually deviate further from the experimental. The reason for this discrepancy is still under investigation.

The modified results at $Re_c = 3.2 \times 10^6$ demonstrate the purpose of the modification well, however the agreement with the experimental results still remains an issue. It can be seen that with the onset modification the results at $FSTI = 0.24\%$ are closer to the LSWT results, but do tend to underestimate the drag coefficient (implying the prediction of transition occurs too far downstream) across the polar. The idea behind the modification was to allow the laminar boundary layer to grow to a larger shape factor before the onset function switches on the production of turbulent kinetic energy (k). It appears though, the modification may allow the laminar boundary layer to develop too much at higher Reynolds numbers and the change of parameter constant will require further investigation.

VI. Conclusion

A roughness amplification model that interacts with the Langtry-Menter transition model has been successfully implemented in the flow solver OVERFLOW-2. Early calibration studies show good agreement with experimental results and confirm the potential of the methodology. Several considerations regarding the impact of freestream turbulence intensity on the Langtry-Menter model were discussed and suggestions presented.

Experimental tests have been carried out at the Texas A&M LSWT using multiple roughness configurations and will be used to further develop and calibrate the roughness amplification model.

Acknowledgments

The effort was performed for Sandia National Laboratories under contract number 1228734 (U.C. Davis) and 1209202 (TAMU) with David Maniaci and Matthew Barone as technical monitors. The work was additionally supported by the National Science Foundation GK-12 RESOURCE program under Grant No. DGE-0948021.

References

[1]Nikuradse, J., "Laws of Flow in Rough Pipes", *NACA Technical Report 1292*, 1933

[2]Braslow, A.L., and Knox, E.C., "Simplified Method for Determination of Critical Height of Distributed Roughness Particles for the Boundary-Layer Transition at Mach Numbers from 0 to 5", *NACA technical report 4363*, 1958.

[3]Corke, T.C., Bar-Sever, A., and Morkovin, M.V., " Experiments on Transition Enhancement by Distributed Roughness", *The Physics of Fluids*, Vol. 29, No. 10, 1986, pp. 3199-3213.

[4]Bons, J.,P., "A Review of Surface Roughness Effects in Gas Turbines" *Journal of Turbomachinery*, Vol. 132, No. 021004, 2010, pp. 1-16.

[5]Kerho, M. F., and Bragg M.,B., "Airfoil Boundary-Layer Development and Transition with Large Leading-Edge Roughness," *AIAA Journal*, Vol. 35, No. 1, Jan. 1997, pp. 75-84

[6]Sareen, A. , Sapre, C.A., and Selig, M.S., "Effects of Leading Edge Erosion on Wind Turbine Blade Performance", *Wind Energy*, DOI: 10.1002/we.1649, 2013.

[7]Berg, D.E., "A Review of the Workshop on WECS Blade-Surface Roughness", *ASME Wind Energy Symposium*, 1993.

[8]van Rooij, R.P.J.O.M., and Timmer, W.A., "Roughness Sensitivity Considerations for Thick Rotor Blade Airfoils", *Journal of Solar Engineering*, Vol. 125, 2003, pp. 468-478.

[9]Dryden, H.L., "Combined Effects of Turbulence and Roughness on Transition", *ZAMP Zeitschrift fr Angewandte Mathematik und Physik*, Vol. 9, No. 5-6, 1958, pp. 249-258.

[10]Merkle, C.L., and Kubota, T., "An Analytical Study of the Effects of Surface Roughness on Boundary-Layer Transition", *Flow Research Inc Technical Report AD/A-004 786*, 1973

[11]Young, A.D., Paterson, J.H., and Jones, J.L., "Aircraft Excrescence Drag", *Aircraft Group for Aerospace Research and Development technical report No. 264*, 1981.

[12]Klebanoff, P.S., and Tidstrom, K.D., "Mechanism by Which a Two-Dimensional Roughness Element Induces Boundary-Layer Transition", *The Physics of Fluids*, Vol. 15, No. 7, 1972, pp. 1173-1186.

[13]Acalar M.S., and Smith, C.R., "A Study of Hairpin Vortices in a Laminar Boundary Layer. Part 1. Hairpin Vortices Generated by a Hemisphere Protuberance", *Journal of Fluid Mechanics*, Vol. 175, 1987, pp. 1-41.

[14]van Ingen, J. L., "The e^N method for transition prediction. Historical review of work at TU Delft," in *38th Fluid Dynamics Conference and Exhibit*, AIAA-2008-3830, June 23-26, 2008, Seattle, Washington.

[15]Brodeur, R. R., and van Dam, C. P., "Transition Prediction for a Two-Dimensional Reynolds-averaged-Navier-Stokes Method Applied to Wind Turbine Airfoils," *Wind Energy* 2001, 4, 61-75.

[16]Mayda, E.A., "Boundary-layer Transition Prediction for Reynolds-averaged Navier-Stokes Methods", Ph.D. Thesis, University of California, Davis, 2007

[17]Menter, F. R., Esch T., and Kubacki, S., "Transition Modeling Based on Local Variables" *Proceedings of the 5th International Symposium on Engineering Turbulence Modelling and Measurement*, Elsevier, Amsterdam, 2002, pp. 555-564.

[18]Langtry, R. B., and Menter, F. R., "A Correlation-Based Transition Model for Unstructured Parallelized Computational Fluid Dynamics Codes," *AIAA Journal*, Vol. 47, No. 12, December 2009, pp. 2894-2906.

[19]Abu-Ghannam, B. J., and Shaw, R., "Natural Transition of Boundary Layers: The Effects of Turbulence, Pressure Gradient, and Flow History," *Journal of Mechanical Engineering Science*, Vol. 22, No. 5, 1980, pp. 213-228.

[20]Van Driest, E.R., and Blumer, C.B., "Boundary Layer Transition: Freestream Turbulence and Pressure Gradient Effects", *AIAA Journal*, Vol. 1, No. 6, 1963, pp. 1303-1306.

[21]Savill, A.M., "Some Recent Progress in Turbulence Modeling of By-pass Transition", Elsevier Sciences Publishers, 1993.

[22]Schubauer, G. B., and Klebanoff, P. S., "Contribution on the Mechanics of Boundary Layer Transition, NACA TN 3489, 1955.

[23]Jespersen, D. C., Pulliam, T. H., and Buning, P. G., "Recent Enhancements to OVERFLOW," *AIAA Paper 97-0644*, Jan. 1997.

[24]Spalart, P.R., and Rumsey, C.L., "Effective Inflow Conditions for Turbulence Models in Aerodynamic Calculations", *AIAA Journal*, Vol. 45, No. 10, 2007, pp. 2544-2558.

[25]Durbin, P.A., Medic, G., Seo, J.M., Eaton, J.K., and Song, S., "Rough Wall Modification of Two Layer $k-\epsilon$", *Journal of Fluids Engineering*, Vol. 123, 2001, pp. 16-21.

[26]Hellsten, A., and Laine, S., "Extension of the $k-\omega$ - SST Turbulence Model for Flows Over Rough Surfaces", *Proceedings of the AIAA Atmospheric Flight Mechanics Conference*, 1997.

[27]Dassler P., Kozulovic D., and Fiala A., "Modeling of Roughness-Induced Transition Using Local Variables", in *V European Conference on Computational Fluid Dynamics*, June 14-17, 2010, Lisbon, Portugal.

[28]Dassler P., Kozulovic D., and Fiala A., "Modeling of Roughness-Induced Transition Using Local Variables", in *European Congress on Computational Methods in Applied Sciences and Engineering (ECCOMAS 2012)*, September 10-14, 2012, Vienna, Austria

[29]E. G. Feindt, "Untersuchungen ber die Abhngigkeit des Umschlages laminar- turbulent von der Oberflchenrauhigkeit und der Druckverteilung", DFL Bericht, 43 (1956)

[30]Beam, R., and Warming, R., "An Implicit Factored Scheme for the Compressible Navier-Stokes Equations," *AIAA Journal*, Vol. 16, No. 4, 1978, pp. 393402

[31]Wilcox, D. C., "Turbulence Modeling for CFD," DCW Industries, Second Edition, La Canada, California 1998.

[32]Kerho, M. F., "Effect of Large Distributed Roughness Near an Airfoil Leading Edge on Boundary-Layer Development and Transition", Ph.D. Dissertation, Dept. of Aeronautical and Astronautical Engineering, Univ. of Illinois at Urbana-Champaign, Urbana, IL, 1995.

[33]Ehrmann, R. S., White, E. B., Maniaci, D. C., Chow, R., Langel, C. M., van Dam, C.P., "Realistic Leading-Edge Roughness Effects on Airfoil Performance" *31st AIAA Applied Aerodynamics Conference* , June 24-27, 2013 , San Diego, California.

[34]Ferrer, E., Munduate., "CFD Predictions of Transition and Distributed Roughness Over a Wind Turbine Airfoil", *47th AIAA Aerospace Sciences Meeting Including The New Horizons Forum and Aerospace Exposition*, AIAA-2009-0269, January 5-8, 2009, Orlando, Florida.

[35]Langtry, R. B., "A Correlation-Based Transition Model Using Local Variables for Unstructured Parallelized CFD Codes," Ph.D. Thesis, Univ. of Stuttgart, Stuttgart, Germany, 2006.

[36]Khayatzadeh, P. and Nadarajah, S., "Laminar-turbulent flow simulation for wind turbine profiles using the $\gamma - \tilde{Re}_{\theta t}$ transition model", *Wind Energy*, DOI: 10.1002/we.1606, 2013, pp. 1-18.